

## Detoxification of copper and zinc from anaerobic digestate effluent by indigenous bacteria: Mechanisms, pathways and metagenomic analysis

Hongbin Yan<sup>a</sup>, Zhiqiang Gu<sup>a</sup>, Qi Zhang<sup>a,\*</sup>, Yunpu Wang<sup>a</sup>, Xian Cui<sup>a</sup>, Yuhuan Liu<sup>a</sup>, Zhigang Yu<sup>b</sup>, Roger Ruan<sup>c</sup>

<sup>a</sup> State Key Laboratory of Food Science and Resources, Engineering Research Center for Biomass Conversion, Ministry of Education, Nanchang University, Nanchang, Jiangxi 330047, PR China

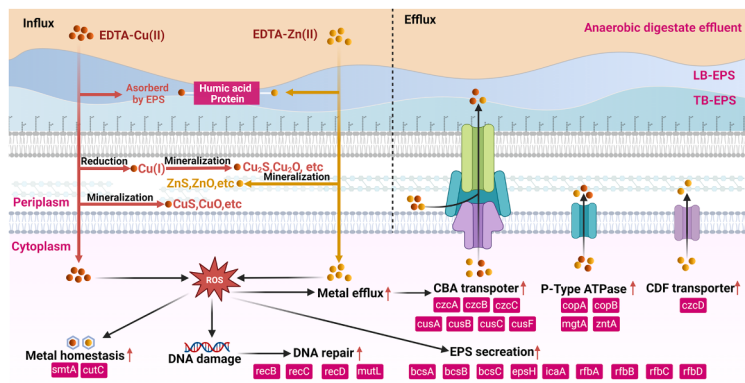
<sup>b</sup> Advanced Water Management Centre, The University of Queensland, Brisbane 4072, Australia

<sup>c</sup> Center for Biorefining and Dept. of Bioproducts and Biosystems Engineering, University of Minnesota, Paul 55108, USA

### HIGHLIGHTS

- Indigenous bacteria were effective in EDTA-complexed Cu(II) and Zn(II) elimination.
- High heavy metals (HMs) concentrations induced ROS generation and EPS secretion.
- Over 50% copper and 60% zinc in bacteria were immobilized on the cell envelope.
- Cu(II) reduction and Zn(II) sulfide precipitation were key detoxification ways.
- Indigenous bacteria upregulated related HMs resistant genes to mitigate HMs stress.

### GRAPHICAL ABSTRACT



### ARTICLE INFO

#### Keywords:

Indigenous bacteria  
Heavy metals removal  
Anaerobic digestate effluent  
Metagenomic analysis

### ABSTRACT

The presence of organic-complexed copper and zinc in anaerobic digestate effluent (ADE) poses persistent ecological toxicity. This study investigated the detoxification performance and biotic responses of indigenous bacteria against ethylene diamine tetraacetic acid (EDTA)-complexed Cu(II) and Zn(II). Heavy metals (HMs) stress induced reactive oxygen species (ROS) generation and enhanced extracellular polymeric substances (EPS) secretion. At a Cu(II) influent concentration of 20.0 mg·L<sup>-1</sup>, indigenous bacteria removed 88.2% of Cu(II) within nine days. The majority of copper and zinc sequestered by bacteria were stored in the cell envelope, with over 50% of copper and 60% of zinc being immobilized. Transmission electron microscopy mapping (TEM-mapping) revealed significant mineralization of copper and zinc on the cell wall. Proteins abundant in EPS, alongside humic acid-like substances, effectively adsorbed HMs. Indigenous bacteria exhibited the capacity to reduce cupric to the cuprous state and cupric is preferentially reduced to cuprous before reaching reducing capacity saturation. Sulfur precipitation emerges as a crucial pathway for Zn(II) removal. Metagenomic analysis indicated that indigenous bacteria upregulated genes related to HMs homeostasis, efflux, and DNA repair, enhancing its

\* Corresponding author.

E-mail addresses: [zhangqi093115@ncu.edu.cn](mailto:zhangqi093115@ncu.edu.cn), [zhangqi09300218@163.com](mailto:zhangqi09300218@163.com) (Q. Zhang).

resistance to high concentrations HMs. This study provided theoretical guidance for employing bacterial consortia to eliminate HMs in complex aquatic environments.

## 1. Introduction

Copper and zinc, two typical heavy metals (HMs), are widely applied as additives in intensive livestock farming for feed and antimicrobial footbaths, result in substantial residues in manure [1–3]. Despite anaerobic digestion (AD) being an environmentally friendly method for converting livestock manure into biogas, it ineffectively removes these metals, leaving considerable amounts of copper and zinc in the anaerobic digestate effluent (ADE). The copper and zinc concentrations in ADE can reach up to 59.4 mg·L<sup>-1</sup> and 234.1 mg·L<sup>-1</sup>, respectively [4]. These residues pose significant risks of environmental pollution, potentially leading to soil and groundwater contamination, bioaccumulation in the food chain, and promotion of antibiotic-resistant genes, thereby limiting ADE's use in agriculture and aquaculture [1,5,6].

The bacteria-based process has attracted increasing interest in recent years for its promising ability in HMs bioremediation, which can remove HMs in various ways, including adsorption, reduction, mineralization, etc. [7,8]. Mejias Carpio et al. (2014) used a heavy metal resistant bacterial consortium as biosorbent to remove copper and achieved a sorption capacity of 450.0 mg·g<sup>-1</sup> dry cells for the consortium [9]. Zhang et al. (2015) applied anaerobic ammonium oxidation granular sludge reactor to remove Cu(II) [10]. The remove efficiency reached 80% in 12 days when the Cu(II) of influent was 5 mg·L<sup>-1</sup>, while high Cu (II) load (12 mg·L<sup>-1</sup>) destroyed the system. Compared with the conventional technologies such as adsorption, electrochemistry, ion exchange, and chemical precipitation, bacteria-based process has several practical advantages, including low cost, more environmentally friendly and more suitable for the treatment of low-concentration HMs wastewater (1–50 mg·L<sup>-1</sup>) [9,11]. Therefore, bacteria-based process is a promising alternative for HMs elimination under stringent discharge limits.

HMs complexation is a non-negligible phenomenon in ADE because AD produces a considerable amount of organic matter, including volatile fatty acids, amino acids, humic acid, and fulvic acid, which can effectively complex copper and zinc [12]. It has been reported that most of the copper and zinc (97–100%) are complexed by organics in ADE [13]. Complexed HMs exhibit enhanced solubility in aqueous environments when compared to their ionic counterparts in free form, and demonstrate stability across a broad spectrum of pH levels, coupled with intricate morphologies. This facilitates their absorption by biological entities, often resulting in a toxicity profile that surpasses that of their free ionic forms [14]. However, current studies have primarily targeted the free HMs; theoretical and practical knowledge about the control of complexed HMs is limited.

This study employed previously isolated indigenous bacteria to treat ADE containing EDTA (ethylene diamine tetraacetic acid)-complexed Cu (II) and Zn(II). We investigated the growth status of indigenous bacteria and analyzed the efficiency of HMs removal, along with their distribution in bacterial components. We explored the removal forms of copper and zinc and identify the functional groups aiding in the removal of these HMs. Changes in the bacterial community's structure and the composition of functional gene at varying HMs concentrations were revealed via metagenomic sequencing. In summary, this study provided a systematic elucidation of the multifaceted response mechanisms of indigenous bacteria to organic-complexed copper and zinc during bioremediation, offering new insights and scientific guidance for bacteria-based process application as a pretreatment process in ADE resource utilization and the management of HMs contaminated wastewater.

## 2. Materials and methods

### 2.1. Anaerobic digestate effluent and indigenous bacteria

ADE was sourced from the waste discharge tank of a pig breeding facility in Pingxiang City, Jiangxi Province, China. It underwent filtration through an eight-layer nylon mesh filter (100 mesh, Tongtai, China) and was preserved at 4 °C for subsequent use. The initial concentrations of Cu(II) and Zn(II) in the ADE, were recorded at 0 mg·L<sup>-1</sup> and 8.1 mg·L<sup>-1</sup>, respectively. Detailed parameters of the ADE were determined and are presented in Table S1. Indigenous bacteria, identified in our prior work [12], was selected for its tolerance to 40 mg·L<sup>-1</sup> Cu(II) and 100 mg·L<sup>-1</sup> Zn(II). It dominantly comprised of five bacterial strains i.e., *Unclassified ug Alcaligenes* (53.80%), *Rhodopseudomonas palustris* (21.30%), *Tisiella praecacuta* (5.10%), *Enterococcus mundii* (4.90%) and *Brevundimonas diminuta* (3.10%). The indigenous bacteria was cultured at 28 ± 1 °C with a light intensity of 3500 Lux to support the photosynthetic *Rhodopseudomonas palustris*.

### 2.2. Stock solution preparation

EDTA, a most commonly used organic chelating agent, was implemented to stabilize Cu(II) and Zn(II), and simulate the organic-complexed copper and zinc in ADE [15]. Stock solutions of Cu(II) and Zn(II) were prepared as described in Text S1.

### 2.3. Experimental design

The experiment utilized 500-mL glass flasks, each filled with 300 mL of sterile ADE. To simulate varying environmental conditions, stock solutions were added to establish a gradient of Cu(II) and Zn(II) concentrations: 1.0 and 10.1 mg·L<sup>-1</sup> (Cu<sub>1</sub>Zn<sub>10.1</sub>); 2.5 and 13.1 mg·L<sup>-1</sup> (Cu<sub>2.5</sub>Zn<sub>13.1</sub>); 5.0 and 18.1 mg·L<sup>-1</sup> (Cu<sub>5</sub>Zn<sub>18.1</sub>); 10.0 mg·L<sup>-1</sup> and 28.1 mg·L<sup>-1</sup> (Cu<sub>10</sub>Zn<sub>28.1</sub>); 20.0 and 48.1 mg·L<sup>-1</sup> (Cu<sub>20</sub>Zn<sub>48.1</sub>); 30.0 and 68.1 mg·L<sup>-1</sup> (Cu<sub>30</sub>Zn<sub>68.1</sub>). The Cu<sub>1</sub>Zn<sub>10.1</sub> means the Cu(II) and Zn(II) concentrations in this group are 1.0 and 10.1 mg·L<sup>-1</sup>, respectively. The serial ratio of Cu(II) and Zn(II) is intended to simulate the condition in ADE, where the Cu(II) concentration is usually one tenth to one half of Zn(II). A control group (Cu<sub>0</sub>Zn<sub>8.1</sub>) featured ADE without additional HMs. Indigenous bacteria was inoculated at a density of 1.0 g·L<sup>-1</sup> (wet weight). Experimental conditions were consistent at 28 ± 1 °C with a light intensity of 3500 Lux, and flasks were manually shaken thrice daily. pH levels were adjusted to maintain a range of 6.0–6.25. The experiment was conducted for a period of 9 days, with all measurements performed in triplicate.

### 2.4. Analytical methods

#### 2.4.1. Indigenous bacterial physiological analysis

The biomass of indigenous bacteria was determined gravimetrically (Text S2). The growth inhibition rate (GI%) of indigenous bacteria was calculated using Eq. (1).

$$GI(\%) = (c_0 - c)/c_0 \quad (1)$$

where  $c_0$  presents the dry biomass weight of the control group at different days,  $c$  presents the dry biomass weight of groups with different initial HMs concentrations at different days.

The supernatant underwent water quality analysis by being filtered using a 0.45 μm membrane. The impact of copper and zinc stress on indigenous bacteria was quantified by measuring reactive oxygen

species (ROS) levels using a reactive oxygen species assay kit (E004-1-1, Nanjing Jiancheng Institute of Biological Engineering, China), following the operating guide. Bacterial viability was determined using the LIVE/DEAD BacLight Bacterial Activity Kit 178 (L7012, Thermo, USA), with procedures and counting methods elaborated in Text S3. Growth dynamics of the bacteria were examined via scanning electron microscope (SEM) analysis with a field emission scanning electron microscope (S-4800, Hitachi, Japan), preparing samples as outlined by Wang et al. (2022) [16] and further detailed in Text S4.

#### 2.4.2. Water quality analysis

The chemical oxygen demand (COD), ammonia nitrogen ( $\text{NH}_4^+$ -N) and total phosphorus (TP) concentration of samples were analyzed using a multi-parameter water quality analyzer (5B-6 C, Lianhua, China). The total carbon (TC), total organic carbon (TOC), inorganic carbon (IC) and total nitrogen (TN) concentration in the samples were analyzed by a TOC/TN analyzer (Multi N/C 3100, Analytik Jena AG, Germany).

#### 2.4.3. Separation of bacterial cellular components

Loosely bound (LB-EPS) and tightly bound extracellular polymeric substances (TB-EPS) were extracted using the thermal extraction method, as outlined by Li and Yang (2007) [17], with procedural specifics provided in Text S5. Following EPS extraction, the residual cells were resuspended in 50 mL of 0.10% NaCl solution and homogenized. The homogenate was subjected to ultrasonic disruption at a power of 50% for 10 min (JY96-IIN, Scientz, China), then centrifuged at 10,000 g for 10 min. The resulting pellet and supernatant were freeze-dried to obtain the cell envelope (cell wall and membrane) and cytoplasm, respectively.

#### 2.4.4. Spatial distribution of copper and zinc

To investigate the spatial distribution of copper and zinc, water samples for quality assessment and suspensions of cellular component were analyzed. Each 5 mL sample was combined with 4 mL of nitric acid ( $\text{HNO}_3$ , analytical reagent grade) and 1 mL of sulfuric acid ( $\text{H}_2\text{SO}_4$ , analytical reagent grade), then digested at 170 °C for 10 min in a microwave digestion system (MDS-6 G, SINEO, CN). The digested samples were subsequently analyzed via Inductively coupled plasma mass spectrometry (ICP-MS, 7800, Agilent Technologies, USA) to quantify copper and zinc concentrations. Additionally, bacterial pellets from the  $\text{Cu}_0\text{Zn}_{8.1}$ ,  $\text{Cu}_5\text{Zn}_{18.1}$  and  $\text{Cu}_{30}\text{Zn}_{68.1}$  groups were isolated, fixed in 2.5% glutaraldehyde at 4 °C, and examined using Transmission electron microscopy mapping (TEM-mapping), adhering to the methodology described in Text S6.

#### 2.4.5. Characterization of cellular components

The content of polysaccharides (PSs) in LB-EPS and TB-EPS was measured using the phenol-sulfuric acid method, employing glucose as a calibration standard. Proteins content (PNs) was determined by measuring the nitrogen content with an elementary analyzer (Vario Micro cube, Elementar, Germany), and applying a conversion factor of 6.25 to estimate protein content. To elucidate the mechanisms behind copper and zinc removal and to identify the forms in which these metals are present within cellular components, we employed a comprehensive suite of analytical techniques. These included Fourier transform infrared spectroscopy (FTIR), Ultraviolet absorption spectrophotometry (UV/Vis), Three-dimension excitation emission matrix fluorescence spectroscopy (3D-EEM), X-ray photoelectron spectroscopy (XPS) and X-ray diffraction (XRD). Detailed descriptions of the instruments and methodological parameters are provided in Text S7.

#### 2.4.6. Metagenomic sequencing analysis

Three parallel harvested bacterial biomass samples of control group ( $\text{Cu}_0\text{Zn}_{8.1}$ ) and high dosage group ( $\text{Cu}_{30}\text{Zn}_{68.1}$ ) were taken on day 9 and stored at -80 °C for further metagenomic sequencing, respectively. The samples were sent to Shanghai Majorbio Bio-Phare Technology Co., Ltd

(Shanghai, China) for Illumina high-throughput sequencing assay (PE150). Metagenomic DNA was extracted using the E.Z.N.A. Soil DNA Kit (Omega, USA). The experimental procedures, including sample quality testing, library construction, library quality testing, and library sequencing, were performed following the guidelines with the standard protocol provided by the manufacturers of the sequencer. The bioinformatic analysis included three major parts: raw data quality control, gene assembly and gene prediction, and species and functional annotation. In brief, the quality control of raw short reads from Illumina sequencing were performed in Fastp 0.20.0. Then the clean short reads were assembled to get contigs with length  $\geq 300$  bp using Megahit 1.1.2. ORF (Open reading frame) prediction of contig was performed using MetaGene (<http://metagene.cb.k.u-tokyo.ac.jp/>). Detailed information of quality control, gene assemble and gene prediction were shown in *Supplemental information*. Databases Kyoto Encyclopedia of Genes and Genomes (KEGG) and Non-Redundant Protein Sequence Database (NR), were used for functional and species annotation, respectively. More data visualizations were performed on Majorbio I-Sanger (<https://cloud.majorbio.com/>). The raw datasets have been submitted to NCBI Sequence Read Archive (SRA) database with the accession number PRJNA1007242.

#### 2.5. Statistical analysis

Most of data analysis and graphing were performed using EXCEL 2019 (Microsoft Office Enterprise, USA), R (v4.1.2), GraphPad Prism 9 (GraphPad Software, USA), and Origin 2023b (OriginLab, USA). All experiments were conducted in triplicate. The significance of  $\alpha$ -diversity indexes and functional genes abundance between different groups were evaluated by the Student's t-test using R package *stats*. The abundance of genes was calculated to reads per kilobase million (RPKM). Principal coordinates analysis (PCoA) based on the Bray-Curtis distance was performed using R package *vegan*.

### 3. Results and discussion

#### 3.1. Growth of indigenous bacteria in response to copper and zinc

As shown in Fig. 1a, the bacterial biomass varied among the control and experimental groups, particularly under high Cu(II) and Zn(II) concentrations ( $\text{Cu}_{20}\text{Zn}_{48.1}$  and  $\text{Cu}_{30}\text{Zn}_{68.1}$ ), demonstrating the inhibitory influence of HMs on indigenous bacterial proliferation. Such an effect was further evidenced by changes in nutrient dynamics within ADE, which vary in accordance with bacterial activity. Specifically, the consumption rates of TOC, TN, and TP, alongside the  $\text{NH}_4^+$ -N production rate, decreased markedly with escalating Cu(II) and Zn(II) levels, underscoring the detrimental impact on bacterial growth (Fig. 1e-h). The inhibition was most pronounced in the  $\text{Cu}_{30}\text{Zn}_{68.1}$  group, where the rate of inhibition surpassed 50% (Fig. 1b). This group also demonstrated significantly elevated ROS levels, indicative of severe bacterial stress due to complexed Cu(II) and Zn(II) (Fig. 1c), aligning with increased cell mortality (Fig. 1d). Cell mortality is an important indicator reflecting the ROS-induced membrane damage [18]. Remarkably, our study revealed that indigenous bacteria could endure environments with up to  $30 \text{ mg L}^{-1}$  Cu(II) and  $68.1 \text{ mg L}^{-1}$  Zn(II), indicating a high maximum tolerated concentration (MTC). On the ninth day, a significant increase in biomass within the  $\text{Cu}_{30}\text{Zn}_{68.1}$  group suggested a potential for these bacterial population to recover to normal levels in subsequent stages.

#### 3.2. Secretion of EPS by indigenous bacteria in response to copper and zinc

Fig. 2 illustrates the effect of Cu(II) and Zn(II) on the variation in TB-EPS and LB-EPS content and composition. EPS secretion showed no significant variation when the dosages of Cu(II) and Zn(II) were equal to or lower than those in the  $\text{Cu}_{10}\text{Zn}_{28.1}$  treatment. However, in the

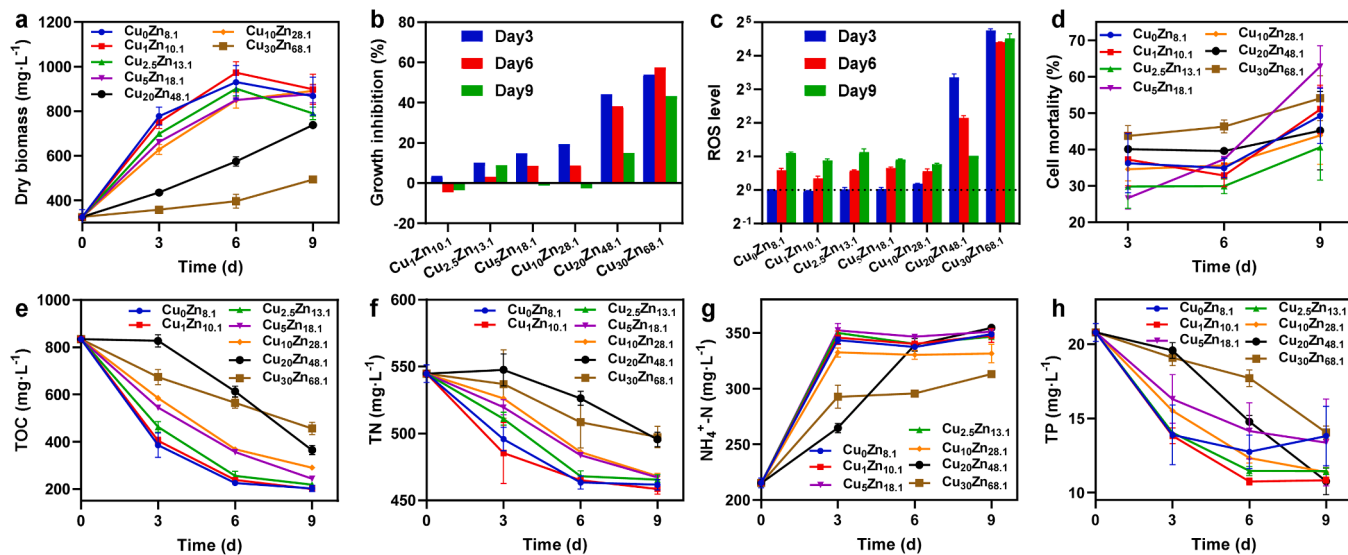


**Fig. 1.** (a) Biomass production. (b) Growth inhibition rate. (c) Cellular ROS level (ROS levels are expressed as a multiple of the cellular ROS concentration on day 3 in the control group, and the y-axis was standardized as binary logarithmic scale). (d) Cell mortality rate. (e-h) Concentration of TOC, TN, TP and  $\text{NH}_4^+$ -N in the ADE over time.

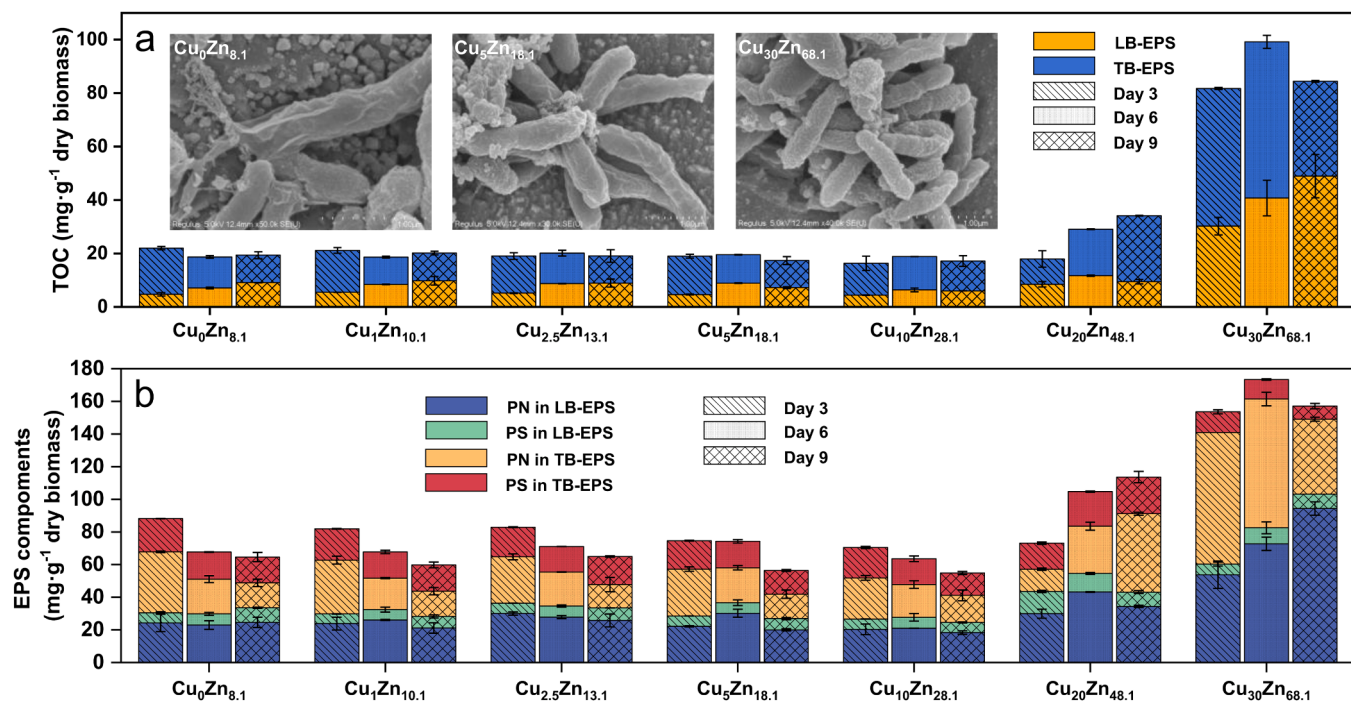


**Fig. 2.** (a) Secretion of TB-EPS and LB-EPS of seven treatments after 3, 6, and 9 days of incubation, and SEM images of indigenous bacteria in  $\text{Cu}_0\text{Zn}_{8.1}$ ,  $\text{Cu}_5\text{Zn}_{18.1}$  and  $\text{Cu}_{30}\text{Zn}_{68.1}$  on day 9. (b) PSs and PNs contents of TB-EPS and LB-EPS.

$\text{Cu}_{20}\text{Zn}_{48.1}$  and  $\text{Cu}_{30}\text{Zn}_{68.1}$  treatments, the content of both TB-EPS and LB-EPS increased substantially, reaching about six times that of the control (Fig. 2a), indicating that high stress from Cu(II) and Zn(II) can trigger more EPS secretion. This was consistent with the cellular ROS level (Fig. 1c). EPS is an extracellular polymer typically secreted by microorganisms, and in the presence of environmental stress, more EPS will be secreted to protect cells [19]. Additionally, SEM images of indigenous bacteria (Fig. 2a) revealed increased EPS secretion, evidenced by more “wrinkles”, known as EPS, appearing on the surface of  $\text{Cu}_{30}\text{Zn}_{68.1}$  compared to the  $\text{Cu}_0\text{Zn}_{8.1}$  and  $\text{Cu}_5\text{Zn}_{18.1}$  treatments. Overall, the indigenous bacteria had a higher TB-EPS content compared to LB-EPS in all groups (Fig. 2a, Fig. S1). When the concentration of Cu(II)

and Zn(II) was equal to or below that of  $\text{Cu}_{10}\text{Zn}_{28.1}$  group, the EPS content was similar, and a slight conversion from TB-EPS to LB-EPS was observed. The main components of EPS are macromolecular substances such as proteins, polysaccharides, and nucleic acids. The PNs and PSs contents of EPS were detected as presented in Fig. 2b, the obtained EPS exhibited considerably higher PNs content compared to PSs. Furthermore, the PNs content in LB-EPS and TB-EPS increased over time, emphasizing the significance of proteins in EPS in resisting HMs stress. This observation aligned with previously reported findings [10,20]. Amino acids, such as aspartic acid and glutamic acid, in proteins can effectively bind to HMs ions to prevent their further entry into the cell, thus preventing toxic effects [20,21].

### 3.3. Removal effect and spatial distribution of copper and zinc

As illustrated in Fig. 3a, influent Cu(II) concentrations of  $5 \text{ mg}\cdot\text{L}^{-1}$  or below can be reduced to under  $1 \text{ mg}\cdot\text{L}^{-1}$  in the effluent aligning with Chinese agricultural irrigation water standard (GB 5084–2021) and the draft of the livestock and poultry wastewater discharge standard (GB18596–2001). Excluding the  $\text{Cu}_{30}\text{Zn}_{68.1}$  group, Cu(II) removal efficiencies surpassed 80% (Fig. 3b), with indigenous bacteria reducing Cu(II) in ADE from  $20.0 \text{ mg}\cdot\text{L}^{-1}$  to  $2.63 \text{ mg}\cdot\text{L}^{-1}$  ( $\text{Cu}_{20}\text{Zn}_{48.1}$ , 86.9%). The  $\text{Cu}_{30}\text{Zn}_{68.1}$  group's diminished bacterial growth led to lower removal efficiency, highlighting biomass's critical role in HMs removal. Previous studies have reported a copper adsorption capacity of  $22.74 \text{ mg}\cdot\text{g}^{-1}\text{-VSS}$  and a copper removal rate of  $67.8 \text{ mg}\cdot\text{g}^{-1}\text{-VSS}$  in anaerobic granular sludge and anaerobic methanation systems, respectively [19,22]. By comparison, the highest Cu(II) removal rate observed in this study was  $23.54 \text{ mg}\cdot\text{g}^{-1}$ -dry biomass, a rate that is comparable to previous findings. For Zn(II), the highest removal efficiency was observed in the

$\text{Cu}_5\text{Zn}_{18.1}$  group (64.9%) (Fig. 3d). Across all experimental groups, Zn(II) removal ranged from 5 to  $13 \text{ mg}\cdot\text{L}^{-1}$ , peaking in the  $\text{Cu}_{10}\text{Zn}_{28.1}$  group. Generally, the Zn(II) removal efficiency attained by indigenous bacteria was less than that for Cu(II), likely due to copper's greater toxicity and bacteria have evolved more effective copper resistance mechanisms.

To understand the removal mechanisms of indigenous bacteria to Cu(II) and Zn(II) stress, the spatial distribution of copper and zinc was analyzed. As illustrated in Fig. 3e and f, the proportion of copper and zinc in bacterial biomass decreased and increased in the ADE with increasing HMs dosages, indicating a saturation point in single-cell absorption capacity. Over time, the increased biomass production facilitated greater copper and zinc transfer into indigenous bacterial cells. Interestingly, the copper and zinc preferentially accumulated in LB-EPS (Fig. 3e and f), despite TB-EPS being more abundant than LB-EPS (Fig. 2a). This can be attributed to the fact that LB-EPS, acting as the outermost protective shield of bacteria, has more opportunities to

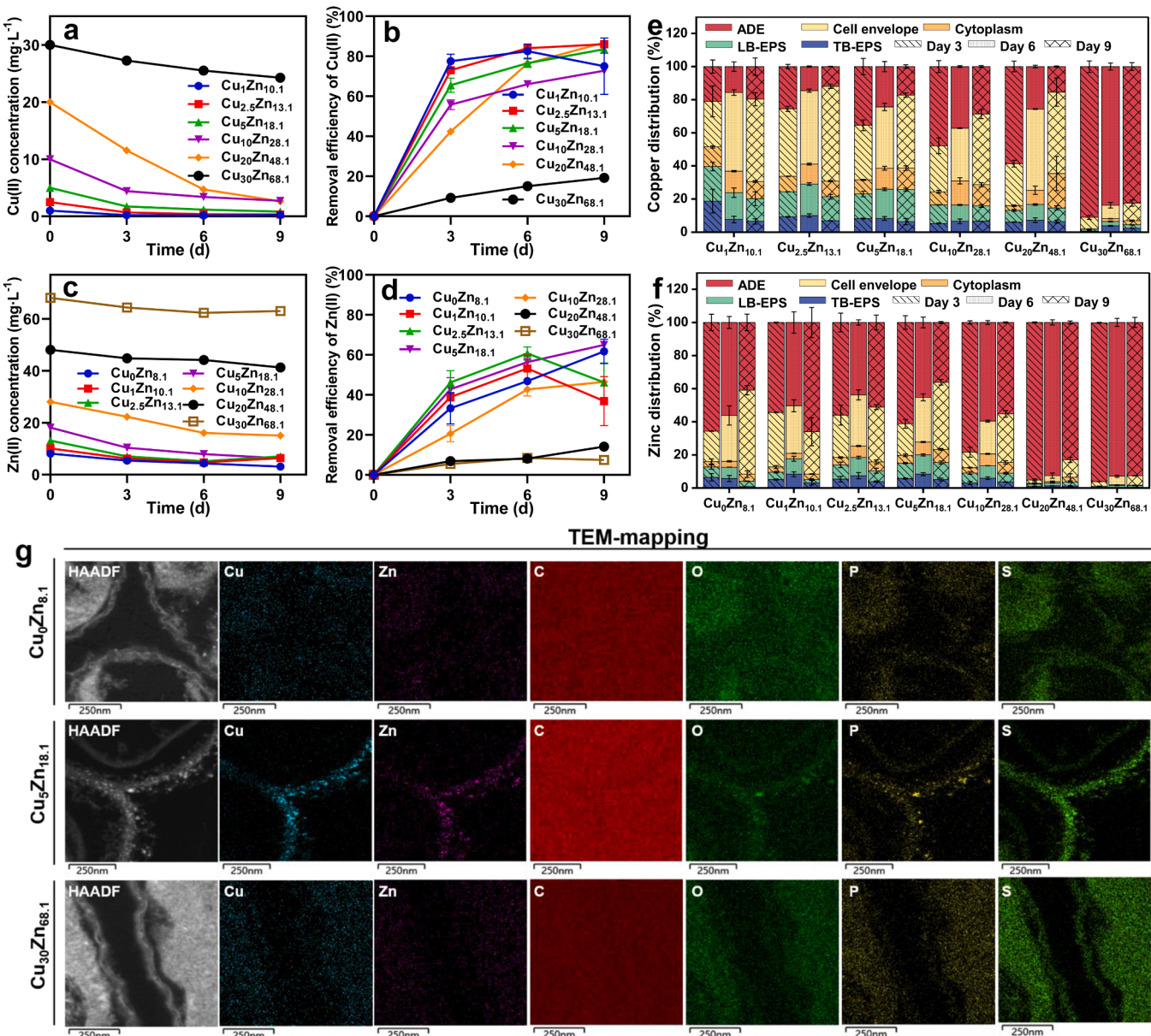


**Fig. 3.** (a) The concentration of Cu(II) in ADE. (b) The removal efficiency of Cu(II). (c) The concentration of Zn(II) in ADE. (d) The removal efficiency of Zn(II). (e) The distribution of copper in the system. (f) The distribution of zinc in the system. (g) TEM-mapping images sampled from indigenous bacterial in  $\text{Cu}_0\text{Zn}_{8.1}$ ,  $\text{Cu}_5\text{Zn}_{18.1}$  and  $\text{Cu}_{30}\text{Zn}_{68.1}$  groups after 9 days incubation.

exchange substances with the ADE. The majority of removed Cu(II) and Zn(II) were localized in the cell envelope, followed by LB-EPS, TB-EPS, and, to a lesser extent, the cytoplasm, which housed less than 20% of these HMs (Fig. S2). The concentrations of copper and zinc in bacterial components showed dynamic migration over time. In the EPS (TB-EPS and LB-EPS) and cytoplasm, the concentration of copper and zinc initially increased and then decreased, while it continued to increase significantly in the cell envelope (Fig. S3 and Fig. S4). Ultimately, the cell envelope is a significant accumulation site, immobilizing over 50% of copper and over 60% of zinc.

We performed TEM-mapping analysis to visualize the spatial distribution of copper and zinc in bacteria. As shown in Fig. 3g, after 9 days incubation, the distribution of copper and zinc overlapped with the oxygen, sulfur and phosphorus in bacteria, indicating that the bacteria had absorbed copper and zinc. Comparing the high angle annular dark field (HAADF) images of TEM with their corresponding mapping images, we observed that copper and zinc were primarily located in the cell wall. Notably, in the HAADF image of  $\text{Cu}_5\text{Zn}_{18.1}$ , two mass-wall-separated cells were presented (Fig. 3g and S5), while the corresponding mapping images showed most of the copper and zinc were located in the cell wall and scarcely in the cell membrane (Fig. 3g and S5). Secondly, minimal copper and zinc were distributed in the cytoplasm and some were distributed in the EPS. These results were consistent with the concentration analysis and demonstrated that copper and zinc mainly removed by the cell wall part of cell envelope. Furthermore, the high-density point (in HAADF image) in the copper and zinc distribution area corresponded to their mineral crystallization (Fig. S6) [8]. It has been reported that the negatively charged cell walls of bacteria aid in immobilizing metals and provide sites for mineral nucleation and

growth [23].

### 3.4. Characterization of cellular components

#### 3.4.1. Chemical state analysis of elements in cellular components

XPS analysis was conducted to determine the chemical state of specific elements (i.e., C, N, O, S, P, Cu, Zn) across various cellular components after 9 days incubation in three distinct groups ( $\text{Cu}_0\text{Zn}_{8.1}$ ,  $\text{Cu}_5\text{Zn}_{18.1}$ ,  $\text{Cu}_{30}\text{Zn}_{68.1}$ ) (Fig. S7). The Cu 2p<sub>3/2</sub> peak at ~932 eV could be attributed to  $\text{Cu}^+$  state of copper, and peak at ~934.5 eV could be assigned to  $\text{Cu}^{2+}$  state of copper [7,24]. As shown in Fig. 4a, no signal of copper was detected in bacterial cells at a Cu(II) dosage of 0 mg·L<sup>-1</sup>, and only  $\text{Cu}^+$  species were found at a Cu(II) dosage of 5 mg·L<sup>-1</sup>. For  $\text{Cu}_{30}\text{Zn}_{68.1}$  group, the Cu(II) dosage was 30 mg·L<sup>-1</sup>, both  $\text{Cu}^{2+}$  and  $\text{Cu}^+$  species were present in each cellular component. This indicated that the Cu(II) removed from ADE by indigenous bacteria was not only eliminated in the form of  $\text{Cu}^{2+}$  but was also accompanied by the reduction of  $\text{Cu}^{2+}$  to  $\text{Cu}^+$  states. And this reduction seems to a prior step as Cu(II) in different components was totally reduced when the Cu(II) dosage lower or equal to 5 mg·L<sup>-1</sup>. In  $\text{Cu}_{30}\text{Zn}_{68.1}$  group, excessive copper in  $\text{Cu}^{2+}$  state take a percentage of 11.0%, 21.28%, 11.51% and 41.08% in LB-EPS, TB-EPS, cell envelope and cytoplasm, respectively. The redox transformation between cupric and cuprous states would induce the production of reactive oxygen radical and improve the cellular ROS level (Fig. 1c) [25]. The O 1s spectra were decomposed into three distinct peaks: inorganic oxygen in metal oxides at ~530 eV, C=O bonds in amide and carboxyl groups at ~532 eV and C-O bonds at ~533 eV (C-O-H of alcohol and carboxyl, C-O-C of ether and ester) (Fig. S8) [26]. The inorganic oxygen in metal oxides may relate to the presence of CuO,

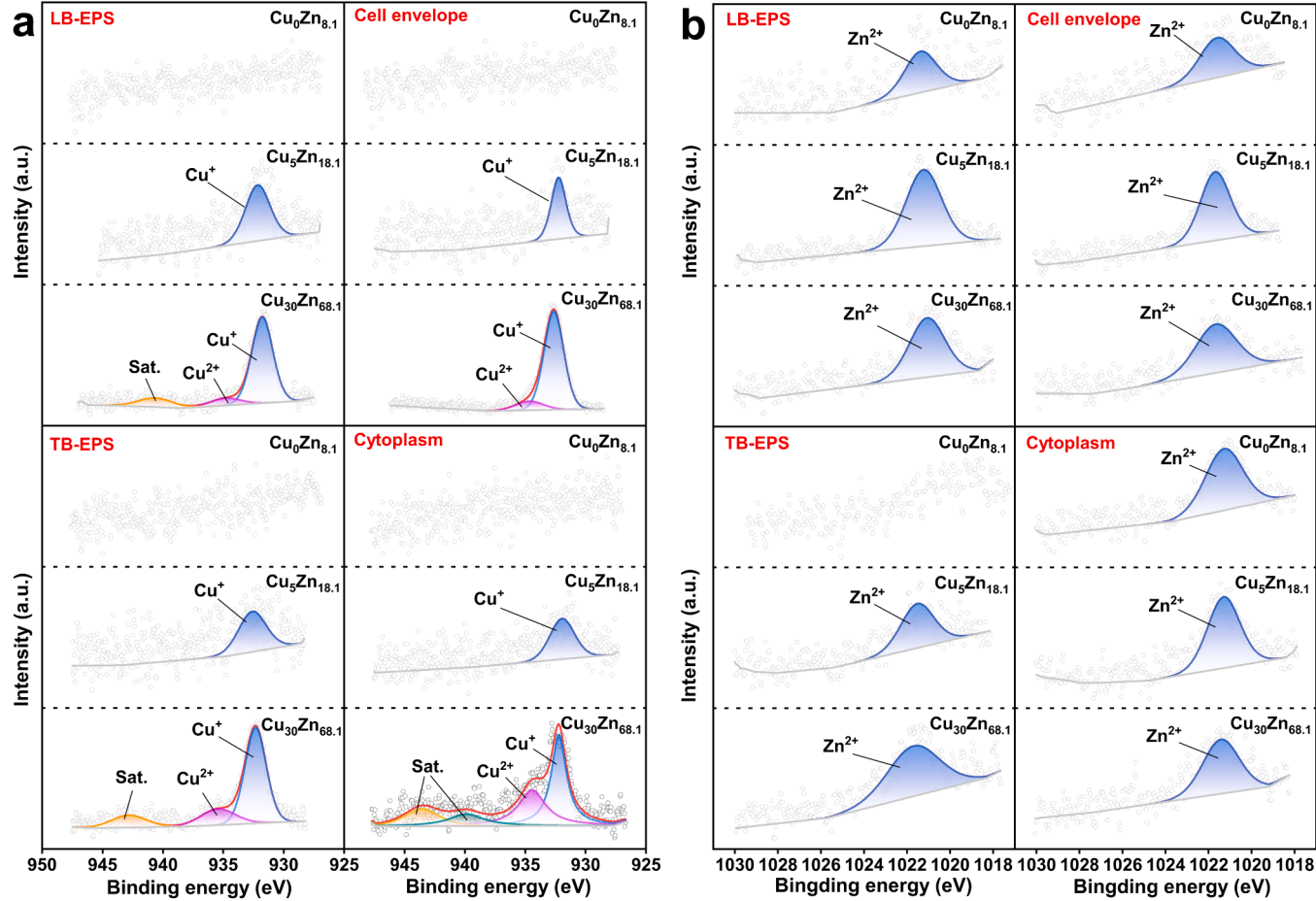


Fig. 4. High-resolution XPS spectra of (a) Cu 2p<sub>3/2</sub> and (b) Zn 2p<sub>3/2</sub> in  $\text{Cu}_0\text{Zn}_{8.1}$ ,  $\text{Cu}_5\text{Zn}_{18.1}$  and  $\text{Cu}_{30}\text{Zn}_{68.1}$  groups after 9 days incubation.

$\text{Cu}_2\text{O}$  and  $\text{ZnO}$  compounds. The peaks of C-O bonds disappeared in cell envelope components when the Cu(II) dosage were  $5 \text{ mg}\cdot\text{L}^{-1}$  and  $30 \text{ mg}\cdot\text{L}^{-1}$ , and the peak intensity decreased with increasing Cu(II) dosage in LB-EPS, TB-EPS and cytoplasm components. This indicated that C-O bond played a crucial role in the reduction process. O-containing groups are effective redox moieties responsible for cupric reduction [7]. The C 1s and N 1s spectra also supported the view, as C 1s peaks at  $\sim 286 \text{ eV}$  contributed to C-O/C-N bounds and N 1s peaks at  $\sim 400 \text{ eV}$  contributed to C-N bonds (Fig. S9 and S10). The Zn 2p<sub>3/2</sub> peak of Zn 2p doublet was shown in Fig. 4b, peaks at about  $1021.5 \text{ eV}$  could be attributed to  $\text{Zn}^{2+}$  state and corresponding to  $\text{ZnS}$ ,  $\text{ZnO}$  and  $\text{Zn}(\text{OH})_2$  compounds [27,28]. All components in different groups showed Zn 2p<sub>3/2</sub> signals excluding the TB-EPS in  $\text{Cu}_0\text{Zn}_{8.1}$ , suggested that TB-EPS has the weakest zinc binding ability.

The P 2p spectra indicated that the form of phosphorus present in all components was phosphate ( $\sim 133.7 \text{ eV}$ , P2p) (Fig. S11) [28], which was consistent with the results of XRD analysis. The S 2p spectra showed two doublet peaks attributed to  $\text{SO}_4^{2-}$  (S 2p<sub>3/2</sub> at  $\sim 168 \text{ eV}$ , S 2p<sub>1/2</sub> at  $\sim 169 \text{ eV}$ ) and  $\text{S}^{2-}$  in metal sulfides (S 2p<sub>3/2</sub> at  $\sim 163 \text{ eV}$ , S 2p<sub>1/2</sub> at  $\sim 164 \text{ eV}$ ) indicated the presence of  $\text{ZnS}$ ,  $\text{CuS}$  and  $\text{Cu}_2\text{S}$  (Fig. S12). Furthermore, XRD patterns showed that  $\text{ZnS}$  diffraction peak was detected in the cell envelope (Fig. S13). Although the medium pH was maintained between 6.0–6.25 to prevent copper and zinc precipitation, proteolysis of bacteria and  $\text{SO}_4^{2-}$  can lead to the production of  $\text{S}^{2-}$  [4]. Additionally, the peak intensity of  $\text{S}^{2-}$  in metal sulfides of cell envelope and cytoplasm greater than that in LB-EPS and TB-EPS (Fig. S12), suggesting that  $\text{S}^{2-}$  plays an important role in precipitation of copper and zinc.

#### 3.4.2. Spectral analysis of cellular components

To elucidate the functional sites responsible for Cu(II) and Zn(II) removal, spectral analyses were also performed. The 3D-EEM spectra, presented in Fig. S14, identified fluorescence organic compounds in cellular components based on the classical region division of fluorescence spectrum (Table S2, Text S8). Peaks for LB-EPS and TB-EPS were associated with humic acid-like and soluble microbial byproduct-like substances. The cell envelope displayed weak fluorescence signals, with traces of aromatic protein-like and fulvic acid-like substances. Peaks in cytoplasm predominantly represented microbial byproduct-like substances, with minor fulvic acid-like signals. Notably, the fluorescence intensity of humic acid-like substances decreased with increasing HMs dosage, indicating their role in HMs sequestration, particularly within TB-EPS and LB-EPS. Despite the absence of humic acid-like substances in the cell envelope, it emerged as the primary site for copper and zinc accumulation, emphasizing the metal-binding efficacy of aromatic protein-like and fulvic acid-like substances. The augmented peak intensity of microbial product-like substances across LB-EPS, TB-EPS, and the cell envelope under metal stress suggested a metabolic shift in bacterial response to Cu(II) and Zn(II). Considering the abundance order of copper and zinc in cellular components (cell envelope > LB-EPS > TB-EPS > cytoplasm), we concluded that the metal binding capacities of cellular organic compounds follow the order: proteins and fulvic acids > humic acids > soluble microbial products (SMPs).

The presence of c-type cytochromes, pivotal in cupric reduction, was inferred from UV-vis spectra, showcasing an absorption peak at  $380$ – $410 \text{ nm}$ , particularly pronounced in the cell envelope (Fig. S15). Additional UV-vis spectra peaks at  $220$ – $300 \text{ nm}$  indicated structural peptides, proteins, aromatic amino acids residues, and humic acids. [29, 30]. The FTIR spectroscopy (Fig. S16) corroborated these findings, with spectra reflecting functional groups such as carboxyl ( $1088$ – $1091 \text{ cm}^{-1}$ ,  $1637$ – $1653 \text{ cm}^{-1}$ ), hydroxyl ( $3440$ – $3450 \text{ cm}^{-1}$ ), carbonyl ( $1637$ – $1653 \text{ cm}^{-1}$ ) and sulfonyl ( $1399 \text{ cm}^{-1}$ ), which effectively bind copper and zinc to achieve the removal purpose [9,31,32]. In addition, the peak at  $520$ – $530 \text{ cm}^{-1}$  indicated the presence of  $\text{PO}_4^{3-}$  and  $\text{S}^{2-}$  in the components, which can interact with copper and zinc to form complexes or precipitates ( $\text{Cu}_3(\text{PO}_4)_2$ ,  $\text{CuS}$ ,  $\text{Cu}_2\text{S}$ ,  $\text{Zn}_3(\text{PO}_4)_2$ ,  $\text{ZnS}$ , etc.) [33].

$1540$ – $1558 \text{ cm}^{-1}$  was a characteristic absorption peak only detected in cell envelope, corresponding to the nitro (-NO<sub>2</sub>), which may be associated with aliphatic or aromatic nitro compounds, aligning with the detection of aromatic protein-like substances primarily in this component.

#### 3.5. Metagenomic analysis

##### 3.5.1. Overview of the microbes inhabiting ADE

To investigate the evolution of bacterial community response to Cu (II) and Zn(II) stress, metagenomic analysis was conducted on the samples taken from  $\text{Cu}_0\text{Zn}_{8.1}$  and  $\text{Cu}_{30}\text{Zn}_{68.1}$  groups after 9 days incubation. The differences of Chao1 and Simpson index (Fig. 5a) between  $\text{Cu}_0\text{Zn}_{8.1}$  and  $\text{Cu}_{30}\text{Zn}_{68.1}$  groups were statistically non-significant (Student's T test's  $p > 0.05$ ), indicating that the rare and dominant species abundance in them were similar. However, the Shannon metric in  $\text{Cu}_{30}\text{Zn}_{68.1}$  was significantly higher than that in  $\text{Cu}_0\text{Zn}_{8.1}$  (Student's T test's  $p < 0.05$ ). This reflected that HMs stress to the indigenous bacteria resulted in a more even microbial structure. Correlation network analysis at the species level revealed an increased tendency for bacterial consortia to form synergistic networks in the  $\text{Cu}_{30}\text{Zn}_{68.1}$  group, suggesting a collective adaptation to mitigate heavy metal stress (Fig. S17).

Gram-negative bacteria constituted the majority of indigenous bacteria (Fig. 5b). PCoA analysis at the species level (Fig. 5c) showed that the microbial compositions of  $\text{Cu}_{30}\text{Zn}_{68.1}$  were different from those of  $\text{Cu}_0\text{Zn}_{8.1}$ . Microbes identified in  $\text{Cu}_0\text{Zn}_{8.1}$  and  $\text{Cu}_{30}\text{Zn}_{68.1}$  exhibited *Proteobacteria* and *Bacteroidetes* dominated structure (Fig. S18). The abundance of *Proteobacteria* decreased in  $\text{Cu}_{30}\text{Zn}_{68.1}$ , especially for *Alphaproteobacteria* (Fig. S19), and *Flavobacteriia* affiliating to *Bacteroidetes* shifted to one of the dominant classes. At the genus level, the abundance of *Rhodopseudomonas* (*Alphaproteobacteria*) decreased significantly from 34% in  $\text{Cu}_0\text{Zn}_{8.1}$  to less than 0.7% in  $\text{Cu}_{30}\text{Zn}_{68.1}$  (Fig. 5e). Instead, an abundance of *Achromobacter* (*Betaproteobacteria*), *Cloacibacterium* (*Flavobacteriia*), *Chryseobacterium* (*Flavobacteriia*), *Pseudomonas* (*Gammaproteobacteria*), and *Lelliottia* (*Gammaproteobacteria*) were significantly enriched in the  $\text{Cu}_{30}\text{Zn}_{68.1}$  group, suggesting they were potential copper and zinc removers and tolerant genera (Fig. 5e).

##### 3.5.2. Functional genes involved in the removal and resistance of copper and zinc

To better understand the resistance mechanism of indigenous bacteria exposed to copper and zinc stress, functional genes were identified and annotated according to the KEGG database. PCoA analysis at the KEGG Orthology (KO) level demonstrated significant alterations in the functional gene composition of bacterial community in  $\text{Cu}_{30}\text{Zn}_{68.1}$  compared to the  $\text{Cu}_0\text{Zn}_{8.1}$  (Fig. 5d). HMs accumulation in living cells typically involves an initial rapid nonspecific uptake and subsequent slower cytoplasm influx, with EPS playing a pivotal role [23]. Bacteria secrete EPS for self-protection, not only against dehydration and toxic substances, but also as a source of carbon and energy under unfavorable conditions [34]. The abundance of genes linked to EPS secretion (*bcsA*, *bcsB*, *bcsC*, *epsH*, *icaA*, *rfbA*, *rfbB*, *rfbC*, *rfbD*) (Fig. 5f) [35] was upregulated (Student's T test's  $p < 0.01$ ), signaling a higher EPS secretion capacity in bacteria exposed to heightened metal levels. It is widely believed that cells prevent ROS generation by reducing free copper ions through intracellular biomolecules [36]. We detected the gene *smtA*, which encodes the SmtA protein whose cysteine residues are able to bind excess cytoplasmic zinc ions [37], and its abundance was significantly higher in  $\text{Cu}_{30}\text{Zn}_{68.1}$  compared to  $\text{Cu}_0\text{Zn}_{8.1}$  (Student's T test's  $p < 0.001$ ). Moreover, *CutC*, a cytoplasmic copper homeostasis protein that binds copper and reduces copper toxicity, is encoded by gene *cutC* and showed an upregulated abundance in  $\text{Cu}_{30}\text{Zn}_{68.1}$  compared to  $\text{Cu}_0\text{Zn}_{8.1}$  (Student's T test's  $p < 0.01$ ). The above detoxification can be called complexation, but for cells that require rapid growth, complexation is energy costly. Therefore, complexation detoxification is only suitable for low concentrations of HMs, and at high concentrations, a

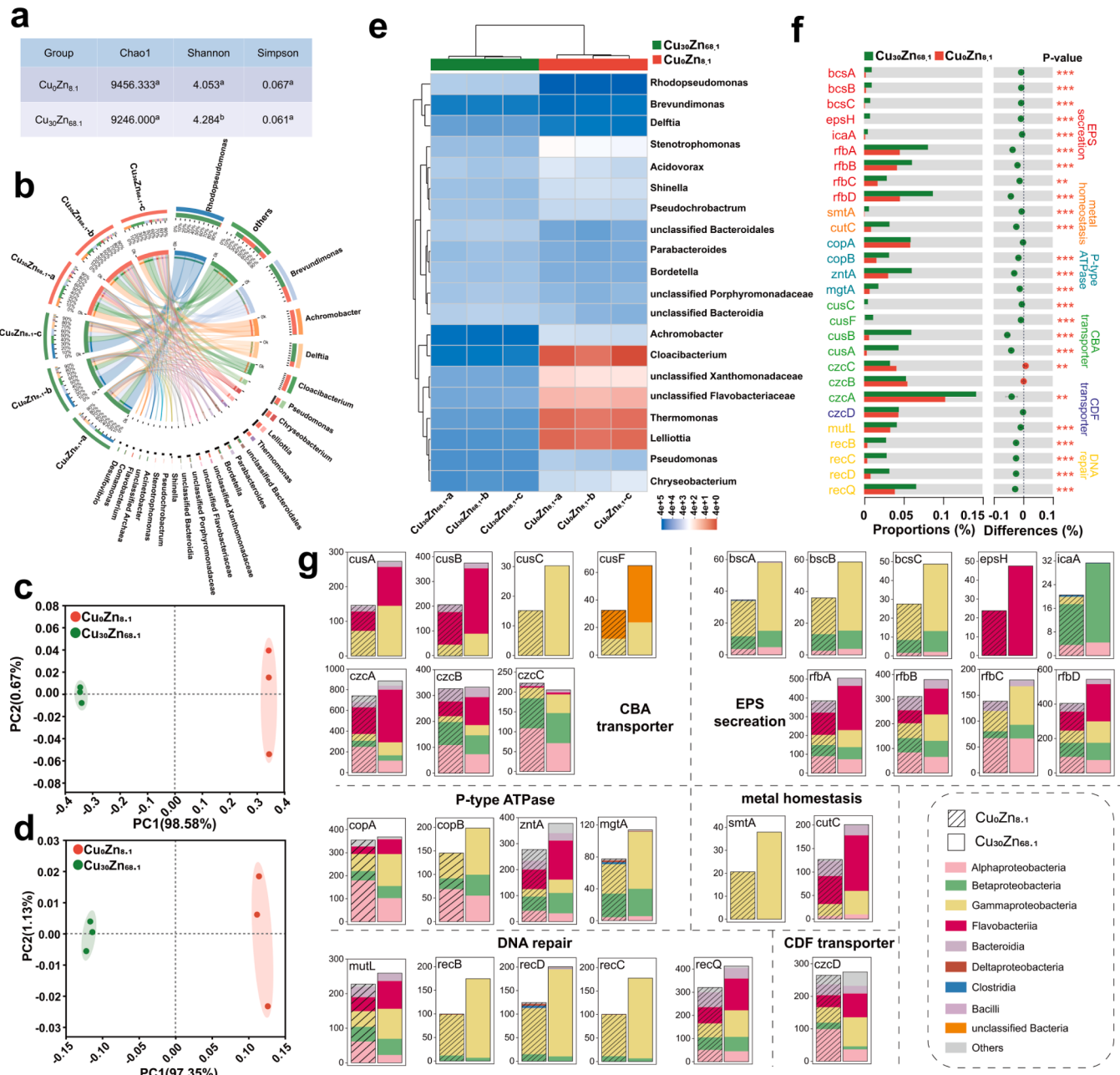


**Fig. 5.** (a)  $\alpha$ -diversity at species level. The superscript letters of numbers indicated the significance of variances estimated from the Student's t-test at a confident level of  $p$ -value  $< 0.05$ . (b) Circos diagram showing bacterial community composition and species abundance at genus level. (c) PcoA analysis for bacterial community composition at species level. (d) PcoA analysis for functional gene composition at KO level. (e) Heatmap of top 20 species abundance at genus level. (f) Abundance of specific functional genes. Asterisks refer to the significance estimated by Student's t-test, \*  $p < 0.05$ , \*\*  $p < 0.01$ , \*\*\*  $p < 0.001$ . (g) Host of corresponding functional genes at the class level.

combination of efflux systems becomes necessary [27].

The microbial HMs efflux system comprises three main types of transport proteins, namely P-Type ATPase, CBA (capsule biogenesis/assembly) transporter and CDF (cation diffusion facilitator) transporter [23]. CopA (encoded by *copA*) and CopB (encoded by *copB*) are two important endosomal copper efflux P-type ATPases that mediate the transport of Cu<sup>+</sup> and Cu<sup>2+</sup> from the cytoplasm to the periplasm, respectively [23]. The abundance of the *copB* was significantly upregulated (Student's T test's  $p < 0.001$ ) and *copA* remained at a high level in the bacterial community of Cu<sub>30</sub>Zn<sub>68.1</sub> compared to Cu<sub>0</sub>Zn<sub>8.1</sub>. ZntA (encoded by *zntA*) and MgtA (encoded by *mgtA*) are two P-type ATPases responsible for Zn<sup>2+</sup> efflux and their abundances were significantly upregulated with increasing metal dosage (Student's T test's  $p < 0.001$ ).

CBA transporter is a transmembrane cellular pump that transports metal ions from the cytoplasm and periplasm outside the cell membrane in Gram-negative bacteria [38]. CusCFBA efflux system is a CBA transporter who controls the efflux of Cu<sup>+</sup> and Ag<sup>+</sup>. CusCFBA system is composed of CusC (an outer membrane factor c (OMF)), CusB (a membrane fusion protein (MFP)), CusA (a resistance-nodulation-division protein (RND protein)) and CusF (periplasmic metallochaperone) [39]. The genes encoding these four proteins, *cusC*, *cusF*, *cusB*, *cusA*, were significantly upregulated in Cu<sub>30</sub>Zn<sub>68.1</sub> compared to Cu<sub>0</sub>Zn<sub>8.1</sub> (Student's T test's  $p < 0.001$ ). CzcCBA, on the other hand, is a CBA transports for Zn<sup>2+</sup> and Cd<sup>2+</sup>, composed of OMF (CzcC), MFP (CzcB) and RND protein (CzcA). It is noteworthy that the CBA system is mainly driven by the RND protein, which is essential for the generation of HMs

resistance [23]. In this study, the gene encoding CzcA, *czcA*, was significantly upregulated in Cu<sub>30</sub>Zn<sub>68.1</sub> compared to Cu<sub>0</sub>Zn<sub>8.1</sub>. CDF transporter is a divalent cation efflux system, are driven by a chemiosmotic gradient formed by protons or potassium, such as CzcD, a key CDF protein, controls the efflux of Zn<sup>2+</sup> and Co<sup>2+</sup> and also regulates the expression of the CzcCBA system [40]. The gene *czcD* (encoding CzcD) is found in indigenous bacterial community and in high abundance. HMs stress causes DNA damage, so DNA repair is also an important pathway for bacteria to resist HMs. Genes related to DNA repair are *mutL*, *recB*, *recC*, *recD* and *recQ* [41,42]. The abundance of all these genes was significantly upregulated in Cu<sub>30</sub>Zn<sub>68.1</sub> compared to Cu<sub>0</sub>Zn<sub>8.1</sub> (Student's T test's *p* < 0.001), indicating a stronger DNA repair ability. Our proposed mechanisms for Cu(II) and Zn(II) removal and resistance by indigenous bacteria was shown in Fig. 6. Additionally, we have investigated the hosts of these key genes. As depicted in Fig. 5g, the predominant hosts at the class level to the above key genes were always *Gammaproteobacteria*, *Betaproteobacteria*, *Alphaproteobacteria*, *Flavobacteria* and *Bacteroidia*. The abundances of the key genes shifted parallelly with the abundance of corresponding microbes, demonstrating that the community of indigenous bacteria is flexible, which can conquer HMs stress by adjusting the abundance of resistance gene-carrying bacteria without reducing the microbial diversity.

#### 4. Conclusion

This study comprehensively investigated an indigenous bacterial process for efficient removal of EDTA-complexed Cu(II) and Zn(II) from ADE, encompassing removal mechanisms, biotic responses and genomic insights. Despite severe growth inhibition and increased ROS generation at high HMs concentrations (Cu(II) + Zn(II): 20.0 + 48.1 mg·L<sup>-1</sup> and 30.0 + 68.1 mg·L<sup>-1</sup>), the indigenous bacteria showed an increasing biomass in nine days, indicating a high HMs tolerance. The highest Zn (II) removal efficiency (64.9%) achieved in Cu<sub>5</sub>Zn<sub>18.1</sub> group, with a Cu (II) removal efficiency of 83.5%. The removal of Cu(II) and Zn(II) involved a combination of functional groups absorption, bioreduction and biomimicry. The aromatic protein-like and fulvic acid-like substances in EPS effectively absorbed HMs. The cell envelope served as the primary accumulation site for both copper and zinc. In the

presence of Cu(II) within ADE, the formation of Cu<sup>+</sup> species was noted in LB-EPS, TB-EPS, the cell envelope, and the cytoplasm, indicative of the copper-reducing capability of indigenous bacteria. Before reaching saturation, the Cu(II) was first reduced to cuprous state and primarily mineralized on cell wall. Conversely, as indigenous bacteria lack the capacity to reduce Zn(II), sulfide precipitation emerged as a critical pathway for the elimination of Zn(II). HMs stress significantly altered both the species structure and functional genes composition of the indigenous bacterial community. Indigenous bacteria acquire resistance by enriching HMs resistance genes carrying bacteria such as *Gammaproteobacteria*, *Betaproteobacteria*, *Alphaproteobacteria*, *Flavobacteria* and *Bacteroidia*. The results of this study can be applied to the control of complexed HMs in other industrial wastewaters.

#### Environmental implication

Copper and zinc, prevalent in livestock farming, accumulate in anaerobic digestate effluent (ADE) in organic-complexed state, posing environmental threats and hindering the resource utilization of ADE. This study presents an innovative bioremediation approach using indigenous bacteria to detoxify ADE. Indigenous bacteria effectively sequester these hazardous metals through intracellular accumulation and extracellular immobilization, reducing environmental pollution and paving the way for safe ADE reuse. This environmentally friendly technology offers a sustainable solution for complexed heavy metals removal from complex aquatic environments, promoting resource circularity and minimizing environmental risks associated with ADE disposal.

#### CRedit authorship contribution statement

**Hongbin Yan:** Writing – original draft, Methodology, Investigation, Formal analysis, Data curation, Conceptualization. **Roger Ruan:** Writing – review & editing, Formal analysis. **Yuhuan Liu:** Writing – review & editing, Conceptualization. **Zhigang Yu:** Investigation, Formal analysis. **Yunpu Wang:** Investigation, Formal analysis. **Xian Cui:** Writing – review & editing, Supervision, Conceptualization. **Zhiqiang Gu:** Writing – review & editing, Supervision, Investigation,

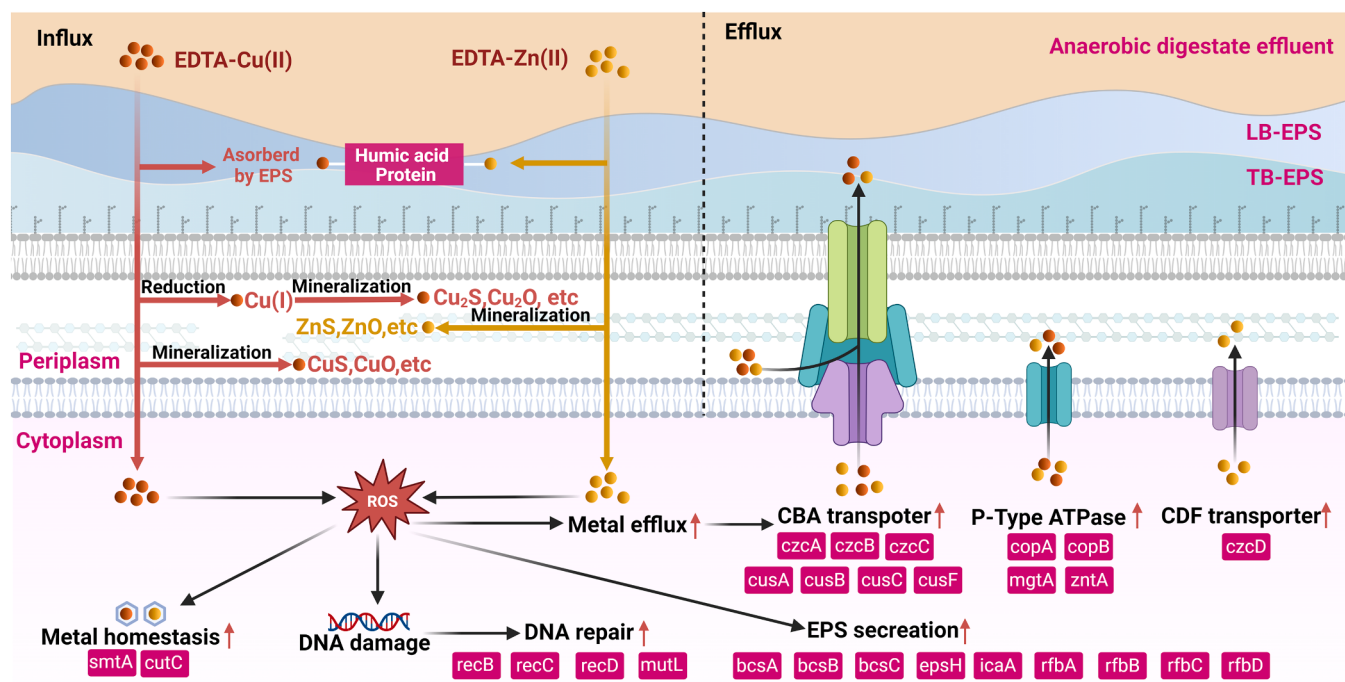


Fig. 6. Proposed mechanisms for Cu(II) and Zn(II) removal and resistance by indigenous bacteria.

Conceptualization. **Qi Zhang:** Writing – review & editing, Resources, Methodology, Formal analysis, Conceptualization.

## Declaration of Competing Interest

The authors declare that they have no known competing financial interests or personal relationships that could have appeared to influence the work reported in this paper.

## Data Availability

Data will be made available on request.

## Acknowledgments

This work was supported by the National Natural Science Foundation of China (No. 22106062), Major Discipline Academic and Technical Leaders Training Program of Jiangxi Province (No. 20225BCJ23026), and Natural Science Foundation of Chongqing (No. CSTB2022NSCQ-MSX0546).

## Appendix A. Supplementary material

Supplementary data associated with this article can be found in the online version at [doi:10.1016/j.jhazmat.2024.133993](https://doi.org/10.1016/j.jhazmat.2024.133993).

## References

- [1] Arya, S., Williams, A., Reina, S.V., Knapp, C.W., Kreft, J.-U., Hobman, J.L., et al., 2021. Towards a general model for predicting minimal metal concentrations co-selecting for antibiotic resistance plasmids. *Environ Pollut* 275, 116602. <https://doi.org/10.1016/j.envpol.2021.116602>.
- [2] Qian, Y., Song, K., Hu, T., Ying, T., 2018. Environmental status of livestock and poultry sectors in China under current transformation stage. *Sci Total Environ* 622–623, 702–709. <https://doi.org/10.1016/j.scitotenv.2017.12.045>.
- [3] Xu, Y., Li, J., OUYANG, Z., Zhang, H., 2021. Implications of feed mineral reduction and enhancement for China's feed standards. *Resour Conserv Recycl* 168, 105342. <https://doi.org/10.1016/j.resconrec.2020.105342>.
- [4] Zeng, Z., Zheng, P., Da, K., Li, Y., Li, W., Dongdong, X., et al., 2021. The removal of copper and zinc from swine wastewater by anaerobic biological-chemical process: performance and mechanism. *J Hazard Mater* 401, 123767. <https://doi.org/10.1016/j.jhazmat.2020.123767>.
- [5] Gu, Z., Yan, H., Zhang, Q., Wang, Y., Liu, C., Cui, X., et al., 2024. Elimination of copper obstacle factor in anaerobic digestion effluent for value-added utilization: performance and resistance mechanisms of indigenous bacterial consortium. *Water Res* 252, 121217. <https://doi.org/10.1016/j.watres.2024.121217>.
- [6] Jankowska, E., Sahu, A.K., Oleśkowicz-Popiel, P., 2017. Biogas from microalgae: review on microalgae's cultivation, harvesting and pretreatment for anaerobic digestion. *Renew Sustain Energy Rev* 75, 692–709. <https://doi.org/10.1016/j.rser.2016.11.045>.
- [7] Xu, H., He, E., Peijnenburg, W.J.G.M., Song, L., Zhao, L., Xu, X., et al., 2021. Contribution of pristine and reduced microbial extracellular polymeric substances of different sources to Cu(II) reduction. *J Hazard Mater* 415. <https://doi.org/10.1016/j.jhazmat.2021.125616>.
- [8] Xu, Z., Chen, Y., Wu, Z., Li, D., Li, X., Feng, X., et al., 2023. Bacterial mineralization of chromium-copper spinel with highly performance in electroplating effluent. *Water Res* 242, 120229. <https://doi.org/10.1016/j.watres.2023.120229>.
- [9] Mejias Carpio, I.E., Machado-Santelli, G., Kazumi Sakata, S., Ferreira Filho, S.S., Rodrigues, D.F., 2014. Copper removal using a heavy-metal resistant microbial consortium in a fixed-bed reactor. *Water Res* 62, 156–166. <https://doi.org/10.1016/j.watres.2014.05.043>.
- [10] Zhang, Z., Deng, R., Cheng, Y., Zhou, Y., Buayi, X., Zhang, X., et al., 2015. Behavior and fate of copper ions in an anammox granular sludge reactor and strategies for remediation. *J Hazard Mater* 300, 838–846. <https://doi.org/10.1016/j.jhazmat.2015.08.024>.
- [11] Ajao, V., Nam, K., Chatzopoulos, P., Spruijt, E., Bruning, H., Rijnarts, H., et al., 2020. Regeneration and reuse of microbial extracellular polymers immobilised on a bed column for heavy metal recovery. *Water Res* 171, 115472. <https://doi.org/10.1016/j.watres.2020.115472>.
- [12] Gu, Z., Liu, Y., Zou, G., Zhang, Q., Lu, R., Yan, H., et al., 2021. Enhancement of nutrients removal and biomass accumulation of *Chlorella vulgaris* in pig manure anaerobic digestate effluent by the pretreatment of indigenous bacteria. *Bioresour Technol* 328, 124846. <https://doi.org/10.1016/j.biortech.2021.124846>.
- [13] Marcato, C.-E., Pinelli, E., Cecchi, M., Winterton, P., Guiresse, M., 2009. Bioavailability of Cu and Zn in raw and anaerobically digested pig slurry. *Ecotoxicol Environ Saf* 72, 1538–1544. <https://doi.org/10.1016/j.ecoenv.2008.12.010>.
- [14] Zhang, Y., Cai, X., Lang, X., Qiao, X., Li, X., Chen, J., 2012. Insights into aquatic toxicities of the antibiotics oxytetracycline and ciprofloxacin in the presence of metal: complexation versus mixture. *Environ Pollut* 166, 48–56. <https://doi.org/10.1016/j.envpol.2012.03.009>.
- [15] Wang, L., Luo, Z., Chelme-Ayala, P., Wei, J., Zhou, X., Min, Y., et al., 2021. The removal of Cu(II)-EDTA chelates using green rust adsorption combined with ferrite formation process. *J Environ Manag* 279. <https://doi.org/10.1016/j.jenman.2020.111516>.
- [16] Wang, Y., Gong, X., Huang, D., Zhang, J., 2022. Increasing oxytetracycline and enrofloxacin concentrations on the algal growth and sewage purification performance of an algal-bacterial consortia system. *Chemosphere* 286, 131917. <https://doi.org/10.1016/j.chemosphere.2021.131917>.
- [17] Li, X., Yang, S., 2007. Influence of loosely bound extracellular polymeric substances (EPS) on the flocculation, sedimentation and dewaterability of activated sludge. *Water Res* 41, 1022–1030. <https://doi.org/10.1016/j.watres.2006.06.037>.
- [18] Hu, Y., Wang, J., Sun, H., Wang, S., Liao, X., Wang, J., et al., 2019. Roles of extracellular polymeric substances in the bactericidal effect of nanoscale zero-valent iron: trade-offs between physical disruption and oxidative damage. *Environ Sci Nano* 6, 2061–2073. <https://doi.org/10.1039/c9en00354a>.
- [19] Li, S., Zhang, C., Li, F., Ren, N.-Q., Ho, S.-H., 2022. Recent advances of algae-bacteria consortia in aquatic remediation. *Crit Rev Environ Sci Technol* 1–25. <https://doi.org/10.1080/10643389.2022.2052704>.
- [20] Wang, Y., Qin, J., Zhou, S., Lin, X., Ye, L., Song, C., et al., 2015. Identification of the function of extracellular polymeric substances (EPS) in denitrifying phosphorus removal sludge in the presence of copper ion. *Water Res* 73, 252–264. <https://doi.org/10.1016/j.watres.2015.01.034>.
- [21] Liu, X., Wu, M., Li, C., Yu, P., Feng, S., Li, Y., et al., 2022. Interaction structure and affinity of zwitterionic amino acids with important metal cations ( $\text{Cd}^{2+}$ ,  $\text{Cu}^{2+}$ ,  $\text{Fe}^{3+}$ ,  $\text{Hg}^{2+}$ ,  $\text{Mn}^{2+}$ ,  $\text{Ni}^{2+}$  and  $\text{Zn}^{2+}$ ) in aqueous solution: a theoretical study. *Molecules* 27, 2407. <https://doi.org/10.3390/molecules27082407>.
- [22] Zhou, X., Chen, C., Wang, A., Jiang, G., Liu, L., Xu, X., et al., 2013. Biosorption of Cu(II) by powdered anaerobic granular sludge from aqueous medium. *Water Sci Technol* 68, 91–98. <https://doi.org/10.2166/wst.2013.228>.
- [23] Pal, A., Bhattacharjee, S., Saha, J., Sarkar, M., Mandal, P., 2022. Bacterial survival strategies and responses under heavy metal stress: a comprehensive overview. *Crit Rev Microbiol* 48, 327–355. <https://doi.org/10.1080/1040841X.2021.1970512>.
- [24] Attar, N., Campos, O.A., Vogelauer, M., Cheng, C., Xue, Y., Schmollinger, S., et al., 2020. The histone H3-H4 tetramer is a copper reductase enzyme. *Science* 369, 59–64. <https://doi.org/10.1126/science.aba8740>.
- [25] Nevitt, T., Öhrvik, H., Thiele, D.J., 2012. Charting the travels of copper in eukaryotes from yeast to mammals. *Biochim Biophys Acta Mol Cell Res* 1823, 1580–1593. <https://doi.org/10.1016/j.bbamcr.2012.02.011>.
- [26] Aissaoui, N., Liaskouciene, I., Genet, M.J., Dupont-Gillain, C., El Kirat, K., Richard, C., et al., 2020. Unravelling surface changes on Cu-Ni alloy upon immersion in aqueous media simulating catalytic activity of aerobic biofilms. *Appl Surf Sci* 503, 144081. <https://doi.org/10.1016/j.japsusc.2019.144081>.
- [27] Nies, D.H., 1999. Microbial heavy-metal resistance. *Appl Microbiol Biotechnol* 51, 730–750. <https://doi.org/10.1007/s002530051457>.
- [28] Xiao, H., Liu, N., Tian, K., Liu, S., Ge, F., 2018. Accelerated effects of nano-ZnO on phosphorus removal by *Chlorella vulgaris*: Formation of zinc phosphate crystallites. *Sci Total Environ* 635, 559–566. <https://doi.org/10.1016/j.scitotenv.2018.04.017>.
- [29] Zhang, Q., Yu, Z., Jin, S., Zhu, L., Liu, C., Zheng, H., et al., 2019. Lignocellulosic residue as bio-carrier for algal biofilm growth: Effects of carrier physicochemical properties and toxicity on algal biomass production and composition. *Bioresour Technol* 293, 122091. <https://doi.org/10.1016/j.biortech.2019.122091>.
- [30] Wang, B.Bin, Shi, X., Liu, X.T., Zou, J.Te, Li, H.J., Peng, D.C., et al., 2019. Insight into the fenton-induced degradation process of extracellular polymeric substances (EPS) extracted from activated sludge. *Chemosphere* 234, 318–327. <https://doi.org/10.1016/j.chemosphere.2019.06.078>.
- [31] Gu, S., Lan, C.Q., 2021. Biosorption of heavy metal ions by green alga *Neochloris oleoabundans*: Effects of metal ion properties and cell wall structure. *J Hazard Mater* 418, 126336. <https://doi.org/10.1016/j.jhazmat.2021.126336>.
- [32] Huang, J., Huang, Z.L., Zhou, J.X., Li, C.Z., Yang, Z.H., Ruan, M., et al., 2019. Enhancement of heavy metals removal by microbial flocculant produced by *Paenibacillus polymyxa* combined with an insufficient hydroxide precipitation. *Chem Eng J* 374, 880–894. <https://doi.org/10.1016/j.cej.2019.06.009>.
- [33] Lin, S., Song, Y., Huo, Y., Wang, Q., Liu, X., Gao, Y., et al., 2021. Cu transport and distribution in different cellular fractions of *Klebsiella oxytoca* strain CAV 1374. *J Hazard Mater* 419. <https://doi.org/10.1016/j.jhazmat.2021.126416>.
- [34] Gupta, P., Diwan, B., 2017. Bacterial exopolysaccharide mediated heavy metal removal: a review on biosynthesis, mechanism and remediation strategies. *Biotechnol Rep* 13, 58–71. <https://doi.org/10.1016/j.btre.2016.12.006>.
- [35] Dueholm, M.K.D., Besteman, M., Zeuner, E.J., Riisgaard-Jensen, M., Nielsen, M.E., Vestergaard, S.Z., et al., 2023. Genetic potential for exopolysaccharide synthesis in activated sludge bacteria uncovered by genome-resolved metagenomics. *Water Res* 229, 119485. <https://doi.org/10.1016/j.watres.2022.119485>.
- [36] Nose, Y., Wood, L.K., Kim, B.-E., Prohaska, J.R., Fry, R.S., Spears, J.W., et al., 2010. Ctr1 is an apical copper transporter in mammalian intestinal epithelial cells in vivo that is controlled at the level of protein stability. *J Biol Chem* 285, 32385–32392. <https://doi.org/10.1074/jbc.M110.143826>.
- [37] Bruins, M.R., Kapil, S., Oehme, F.W., 2000. Microbial resistance to metals in the environment. *Ecotoxicol Environ Saf* 45, 198–207. <https://doi.org/10.1006/eesa.1999.1860>.

- [38] Prabhakaran, P., Ashraf, M.A., Aqma, W.S., 2016. Microbial stress response to heavy metals in the environment. *RSC Adv* 6, 109862–109877. <https://doi.org/10.1039/C6RA10966G>.
- [39] Bagai, I., Liu, W., Rensing, C., Blackburn, N.J., McEvoy, M.M., 2007. Substrate-linked conformational change in the periplasmic component of a Cu(I)/Ag(I) efflux system. *J Biol Chem* 282, 35695–35702. <https://doi.org/10.1074/jbc.M703937200>.
- [40] Montanini, B., Blaudez, D., Jeandroz, S., Sanders, D., Chalot, M., 2007. Phylogenetic and functional analysis of the Cation Diffusion Facilitator (CDF) family: improved signature and prediction of substrate specificity. *BMC Genom* 8, 107. <https://doi.org/10.1186/1471-2164-8-107>.
- [41] Dillingham, M.S., Kowalczykowski, S.C., 2008. RecBCD enzyme and the repair of double-stranded DNA breaks. *Microbiol Mol Biol Rev* 72, 642–671. <https://doi.org/10.1128/MMBR.00020-08>.
- [42] Yamamoto, T., Iino, H., Kim, K., Kuramitsu, S., Fukui, K., 2011. Evidence for ATP-dependent structural rearrangement of nuclelease catalytic site in DNA mismatch repair endonuclease MutL. *J Biol Chem* 286, 42337–42348. <https://doi.org/10.1074/jbc.M111.277335>.